Microfluid Nanofluid
DOI 10.1007/s10404-011-0835-0

RESEARCH PAPER

Focusing microparticles in a microfluidic channel with ferrofluids

Taotao Zhu · Rui Cheng · Leidong Mao

Received: 5 May 2011 / Accepted: 14 June 2011

Abstract We report a novel on-chip microparticles focusing technique using stable magnetic nanoparticles suspension (i.e., ferrofluids). The principle of focusing is based on magnetic buoyancy forces exerted on non-magnetic particles within ferrofluids under non-uniform magnetic field. The design, modeling, fabrication, and characterization of the focusing scheme are presented. Focusing of 4.8, 5.8, and 7.3 μm microparticles at various flow rates are demonstrated in a microfluidic channel. Our scheme is simple, low-cost, and label-free compared to other existing techniques.

Keywords Focusing · Ferrofluid · Magnetic buoyancy force

1 Introduction

Over the past decade, microfluidic devices have been increasingly used to manipulate particles and cells owing to their reduced sample consumption, low-cost, small footprints, and other advantages (Whitesides 2006; Pamme 2007; Tsutsui and Ho 2009; Gossett et al. 2010). Among various manipulation operations, focusing microparticles into a narrow stream becomes a critical step in these devices in order to enable downstream analytical procedures. For example, in miniaturized flow cytometry schemes, fluorescently or magnetically labeled microparticles (both synthetic and biological) need to be focused into a tiny volume to permit accurate counting and sorting. Many microfluidic particle-focusing techniques have been developed for such application, including the ones using hydrodynamic sheath flow (Lee et al. 2006; Kummrow et al. 2009), electrokinetic sheath flow (Xuan and Li 2005), optical force (Zhao et al. 2007), dielectrophoretic force (Wang et al. 2007; Zhu and Xuan 2009), and acoustic force (Petersson et al. 2005; Shi et al. 2008), as detailed in three excellent reviews by Huh et al. (2005), Chung and Kim (2007), and Xuan et al. (2010).

Using magnetic force for microparticles manipulation (Liu et al. 2007) and focusing (Afshar et al. 2011) provides an attractive alternative to the above-mentioned techniques. Functionalized magnetic beads of various sizes (typically several microns in diameter) can be used to specifically transport particles and cells from solution using a simple magnetic setup with great controllability and reliability (Pamme 2006; Liu et al. 2009; Gijs et al. 2010). It is estimated that magnitude of magnetic forces on microparticles can be as high as nanoNewtons (Liu et al. 2009; Gijs et al. 2010). Commonly used magnetic materials, for example, iron oxides have minimal interferences with biological and chemical processes of samples (Adair 1991; Pankhurst et al. 2003, 2009; Krishnan 2010). Furthermore, magnetic manipulation can be implemented with the aid of simple permanent magnets or electromagnets, rendering the cost and integration effort of systems lower. However, the downside is that this label-based technique is manually intensive and goes contrary to the trend of miniaturization and integration in microfluidic systems. There are also issues of removing magnetic labels from samples prior to further analysis. Finally, magnetic moments of these beads, even from the same batch, can vary

T. Zhu
Department of Chemistry, Nanoscale Science and Engineering Center, The University of Georgia, Athens, GA 30602, USA

R. Cheng · L. Mao (✉)
Faculty of Engineering, Nanoscale Science and Engineering Center, The University of Georgia, Athens, GA 30602, USA
e-mail: mao@uga.edu

Published online: 24 June 2011

dramatically due to manufacturing procedures, making scaling of this technique problematic (Mihajlovic et al. 2007; Shevkoplyas et al. 2007).

Recently, a new approach to magnetically manipulate non-magnetic microparticles has been developed using magnetic fluids, including paramagnetic salt solutions and ferrofluids (Yellen et al. 2005; Kose et al. 2009). The purpose of using magnetic fluids is to induce an effective magnetic dipole moment within a non-magnetic object. Under non-uniform magnetic field, particle will experience a magnetic buoyancy force, analogous to buoyancy force, as magnitude of the force is proportional to volume of the particle. This principle was used to demonstrate continuous particle focusing and separation with paramagnetic salt solutions in microfluidic devices (Peyman et al. 2009; Rodriguez-Villarreal et al. 2011). However, magnetic susceptibility of such a paramagnetic salt solution is about 5 orders of magnitude weaker than that of a typical ferrofluid. For example, 1 M concentration of $MnCl_2$ has a susceptibility of $\sim 10^{-6}$, while a ferrofluid with 5–10% volume ratio has a susceptibility of 1 (Rosensweig 1985). Such low susceptibility of paramagnetic salt solutions often translates to slower focusing speed and lower throughput.

Ferrofluids are colloidal suspensions of magnetic nanoparticles (Rosensweig 1985). The nanoparticles, normally magnetite (Fe_3O_4) with approximately 10 nm diameter are covered by surfactants to keep them apart, and suspended within a compatible liquid medium. Magnetic susceptibility of a typical ferrofluid is at least five orders larger than that of a paramagnetic salt solution, rendering fast and high-throughput manipulation of microparticles possible. Non-magnetic particles within ferrofluids, experiencing a magnetic buoyancy force under non-uniform magnetic fields, can be manipulated in the weaker field direction, enabling various applications including size-based separation and trapping (Yellen et al. 2005; Kose et al. 2009; Zhu et al. 2010). In this study, we introduce a novel microfluidic particle-focusing scheme, involving manipulation of microparticles within ferrofluids via external magnetic fields. A schematic of the prototype device using a PDMS channel fabricated by standard soft lithography is shown in Fig. 1a. A pair of Neodymium–Iron–Boron (NdFeB) magnets, with their magnetizations facing each other, are embedded in opposite sides of the PDMS channel, creating a large magnetic field gradient between edges of the magnets and center of the microfluidic channel. Microparticles and ferrofluid mixture solutions are injected into the microfluidic channel by a pressure-driven flow. Once entering the region between magnets, deflections of non-magnetic particles from their laminar flow paths occur because of the magnetic buoyancy forces. Magnitudes of the force are proportional to the volume of particles. Counter-acting hydrodynamic drag force, on the other hand, scales with the diameter of the particles. This observation was used to continuously focus non-magnetic particles in a microfluidic channel with ferrofluids.

2 Materials and methods

PDMS microfluidic channel was fabricated through a standard soft-lithography approach and attached to a flat surface of another piece of PDMS layer. Masks of channel pattern were created using AutoCAD 2008 (Autodesk Inc., San Rafael, CA) and printed by a commercial photo-plotting company (CAD/Art Services Inc, Bandon, OR).

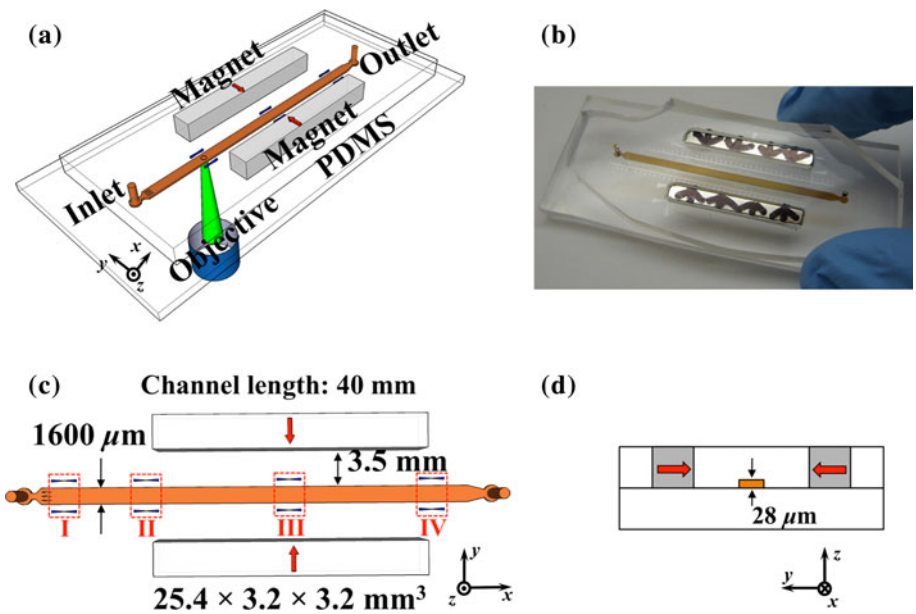

Fig. 1 **a** Schematic representation of the focusing device with permanent magnets and a microfluidic channel. **b** An image of the fabricated device. **c** *Topview* of the system and locations of the observation windows. *Arrows* indicate the direction of magnet's magnetization. The origin of coordinate system is at the center of the microchannel. **d** Cross-section of the system

Dimensions of the microfluidic channel are listed in Fig. 1. Thickness of the channel was measured to be 28 μm by a profilometer (Dektak 150, Veeco Instruments Inc., Chadds Ford, PA). Before attachment PDMS surfaces were treated with plasma (PDC-32G plasma cleaner, Harrick Plasma, Ithaca, NY) at 11.2 Pa O_2 partial pressure with 18 W power for 1 min. NdFeB magnets were incorporated into the device during PDMS curing step. Figure 1b shows a fabricated device used in our study.

We used a commercial water-based magnetite ferrofluid (EMG 408, Ferrotec Co., NH) in our experiments. Volume fraction of magnetite particles for this particular ferrofluid is 1.1%. Mean diameter of nanoparticles has been determined from Transmission electron microscopy images to be 10.2 nm. Initial magnetic susceptibility was measured to be 0.26; saturation magnetization (μ_0M) was 60 Gauss; viscosity was 1.2×10^{-3} kg/m s. This ferrofluid was mixed with 0.1% Tween 20 (5% w/w) to prevent potential particles aggregation during experiments. Fluorescent spherical microparticles (4.8, 5.8, and 7.3 μm in diameter, Thermo Fisher Scientific Inc., Waltham, MA) were mixed with ferrofluids to observe focusing effects. Flow experiment was conducted on the stage of an inverted microscope (Zeiss Axio Observer, Carl Zeiss Inc., Germany). During experiments, ferrofluid and microparticles mixture into microchannel were maintained at tunable flow rates using a syringe pump (Nexus 3000, Chemyx Inc., Stafford, TX). Two NdFeB permanent magnets were used to produce required magnetic fields for focusing. Saturation magnetizations of both magnets were measured to be 0.8 T by a Gauss meter (Model 5080, Sypris, Orlando, FL) and an axial probe with 0.381 mm diameter of circular active area. The images of particles stream were recorded using a CCD camera (SPOT RT3, Diagnostic Instruments, Inc., Sterling Heights, MI) and analyzed in ImageJ software.

We have previously developed a 2D analytical model for transports of non-magnetic particles within ferrofluids in a microfluidic system (Zhu et al. 2011). In this study, we extend our analytical model to enable fast and accurate predications of microparticle trajectories in all three dimensions. We choose analytical model over numerical ones due to the consideration of simulation speed and accuracy. The accuracy of numerical approaches depends heavily on their mesh quality. They are time-consuming and not suitable for parametric studies aimed for quick device design and optimization. In brief, we obtain 3D microparticle trajectories in microchannels by (1) calculating magnetic buoyancy force on particles using a 3D analytical model of magnetic field distribution and a nonlinear magnetization model of ferrofluids inside microchannel, (2) deriving and solving governing equations of motion for particles in laminar flow condition using analytical expressions of dominant magnetic buoyancy and hydrodynamic drag forces. Experimental measurements using a Gauss meter confirm the validity of our analytical model of magnetic field distributions.

3 Results and discussions

Figure 2 depicts simulation results of distributions of magnetic field and magnetic force within the microchannel, as well as representative trajectories of 4.8 μm microparticles at different flow rates in all three dimensions. For example, surface plot in Fig. 2a shows magnitude of magnetic fields of x–y plane at $z = 0$ within the channel. From boundaries to center of the channel, magnitude of magnetic fields decays quickly, eventually forming a local magnetic field minimum at center of the channel. Consequently, microparticles experience magnetic buoyancy forces pointing toward the field minimum direction once entering the channel, as shown in Fig. 2b. The force is computed on a 4.8 μm particle and magnitude of the force is on the order of 1 picoNewton. Note that magnitude of magnetic buoyancy force can be further increased to nanoNewtons range by replacing current ferrofluids with more concentrated ones, using microparticles with larger diameters, and creating a greater magnetic field gradient. Streams of microparticles can be quickly focused by magnetic buoyancy force toward center of the channel, balanced by hydrodynamic drag force, with a mean speed depending on the applicable flow rates. Figure 2c shows relationship between the focusing effect and particle flow rates. Naturally, microparticles are much more focused with slower flow rate, which corresponds to a longer residual time within the channel. The x-component of magnetic buoyancy force changes its polarity around the edges of magnets. Microparticles to the left of magnets experience x-direction deceleration and move slower than the speed of fluids; particles to the right of the magnet experience x-direction acceleration and move faster than the speed of fluids. Figure 2d–f illustrate distributions of magnetic field and force, as well as trajectories of microparticles of y–z plane at $x = 0$ within the channel; Fig. 2g–i illustrate the cases of x–z plane at $y = 0$. We extend our previous 2D analytical model into 3D in this work, in part due to the opaqueness of ferrofluids (Rosensweig 1966) and its negative impact on observation of particles motion. It is a less of a problem when diluted ferrofluids ($\sim$1% v/v) and thin microchannel are used. However, with a concentrated ferrofluid ($\sim$10% v/v) in a thick microchannel, fluorescent microparticles are visible only when they are very close ($\sim$1 μm) to surfaces of the channel. For that reason, we are interested in knowing the motion of microparticles in z-direction. It becomes obvious that the relative position of magnets and channel play a dominant

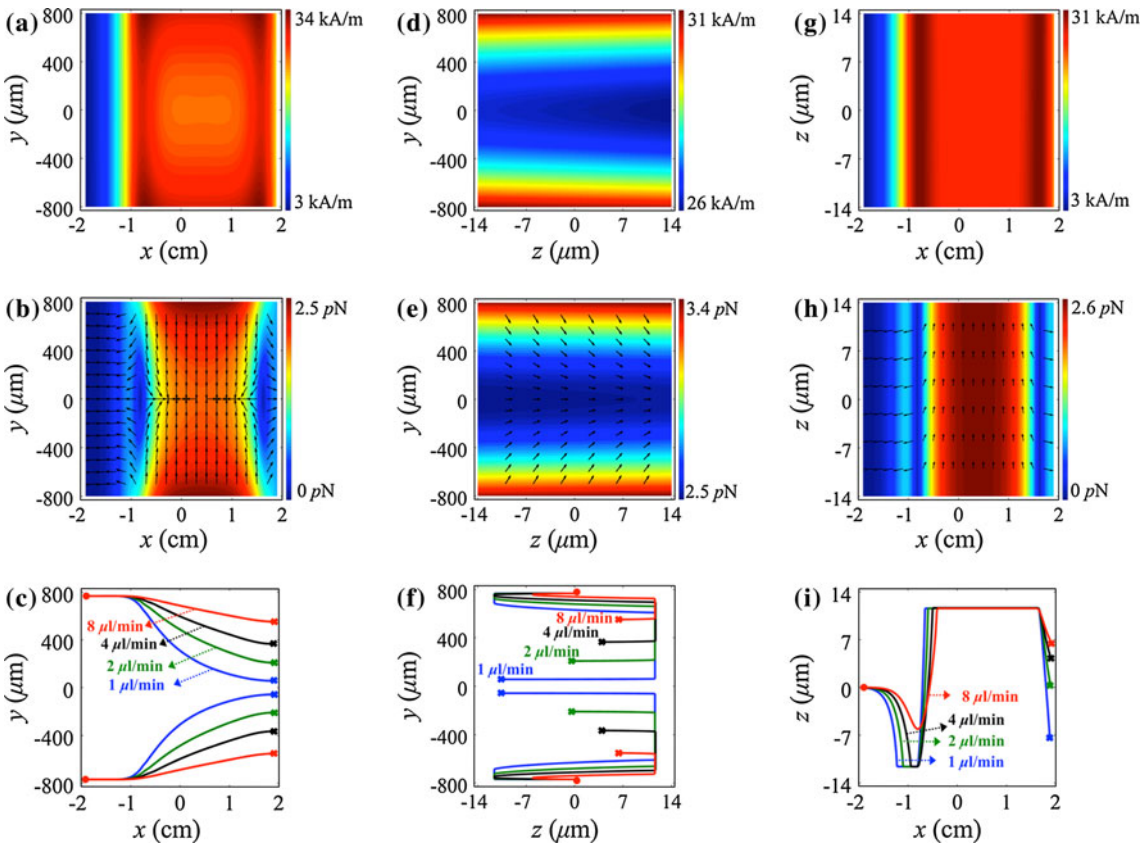

Fig. 2 Analytical simulation of magnetic field and force distributions in the microfluidic channel and trajectories of microparticles (4.8 μm in diameter) at different flow rates. Simulation parameters match experimental conditions. **a–c** x–y plane ($z = 0$), **d–f** y–z plane ($x = 0$), **g–i** x–z plane ($y = 0$) of magnetic field strength (surface plot) (**a**, **d**, **g**), magnetic force (surface plot: force magnitude; *arrow* plot: force direction) (**b**, **e**, **h**), and particles' trajectories at different flow rates (**c**, **f**, **i**). *Dots* indicate starting points, while *crosses* indicate ending points of particles' trajectories

role in determining vertical displacements (z) of particles. Simulation results from Fig. 2f and i indicate in our current experimental setup all particles were quickly pushed toward one of the channel surfaces, depending on their locations in x-direction. We observed in flow experiments that most of the particles were pushed onto bottom surface of the channel as soon as they entered the channel. Furthermore, our analytical model can enable fast and accurate study of 3D particle-focusing effects in microchannels.

Figure 3 shows distributions of fluorescent microparticles (4.8, 5.8, and 7.3 μm) that were recorded during the focusing process at two different flow rates (1 and 8 μl/min) in four different observation windows marked as I, II, III, and IV in Fig. 1c. For example, Fig. 1a depicts the focusing of 4.8 μm particles at 1 μl/min flow rate. Window I was to the left of permanent magnets, therefore microparticles barely experienced magnetic buoyancy forces in this area, as evident in simulation results of Fig. 1b. Consequently, the distribution of microparticles in this area was uniform across the width of the channel. As microparticles entered the area in which the magnetic buoyancy force becomes dominant (window II), the force exerted on the particles drove them toward the centerline of the channel, where magnetic field minimum existed. As the particles entered window III, they were focused into a narrow stream in the middle of the channel. At window IV, the width of the particle stream was measured to be approximately 200 μm, about one-eighth of the channel width.

As we mentioned earlier, the focusing effect of microparticles is greater with slower flow rate, as demonstrated by experimental comparisons between 1 and 8 μl/min in Fig. 3. We also observed that the focusing effect was dependent upon diameter of the microparticles—the larger the particles, the greater the focusing effect. This dependence can be explained through a simple force analysis. Magnetic buoyancy force is proportional to the volume of the particle, while hydrodynamic viscous drag scales only with the diameter. Therefore, particle migration in the y-direction balanced by both magnetic buoyancy and hydrodynamic drag force depends on the square of particle diameter. In order to compare simulation and experimental results, we obtained trajectories of microparticles in a

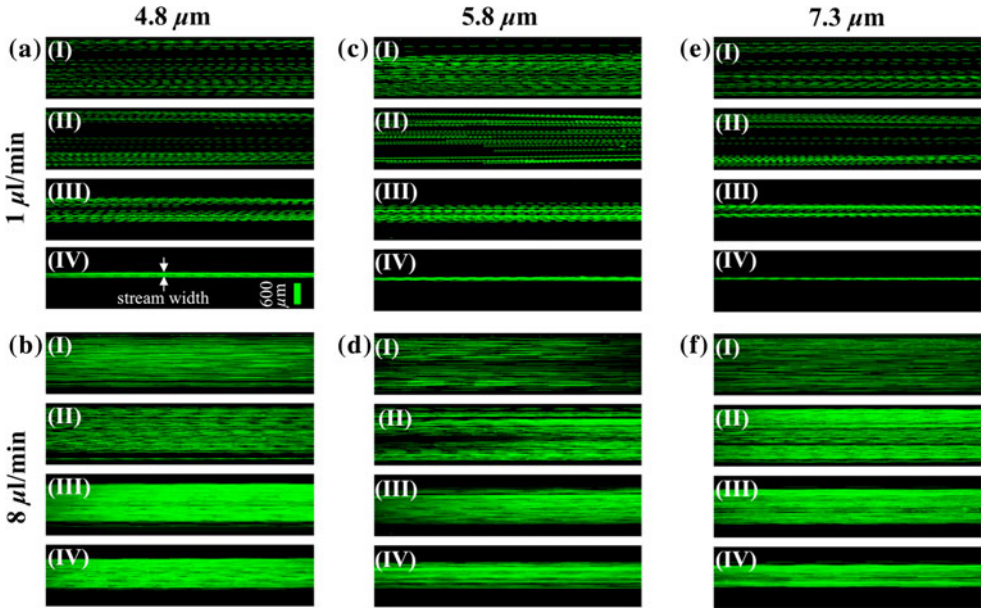

Fig. 3 Experimental composite fluorescent images of observation windows (*I–IV*) for 4.8 μm (**a**, **b**), 5.8 μm (**c**, **d**), 7.3 μm (**e**, **f**) particles at 1 μl/min (**a**, **c**, **e**) and 8 μl/min (**b**, **d**, **f**) flow rates. Widths of particles stream are used to calculate the contraction ratios depicted in Fig. 4

microfluidic system depicted in Fig. 1a using the 3D analytical model described in previous section. Specifically, we simulated spherical particles with 4.8, 5.8, and 7.3 μm diameters in a channel with flow rate varied from 1 to 8 μl/min. Other simulation parameters, including dimensions of channel and magnets, saturation magnetization of magnets, properties of fluids, were chosen to match the exact experimental conditions. Experimental stream widths were obtained by measuring the width particle stream at windows II, III, and IV in Fig. 1c. Contraction ratio is defined as the width of particles stream in window II over the one in window IV. In Fig. 4, predicted stream width and contraction ratio show a reasonable agreement with experimental data, confirming the validity of our analytical model. We do observe slight discrepancy between theoretical and experimental results, which may be attributed to

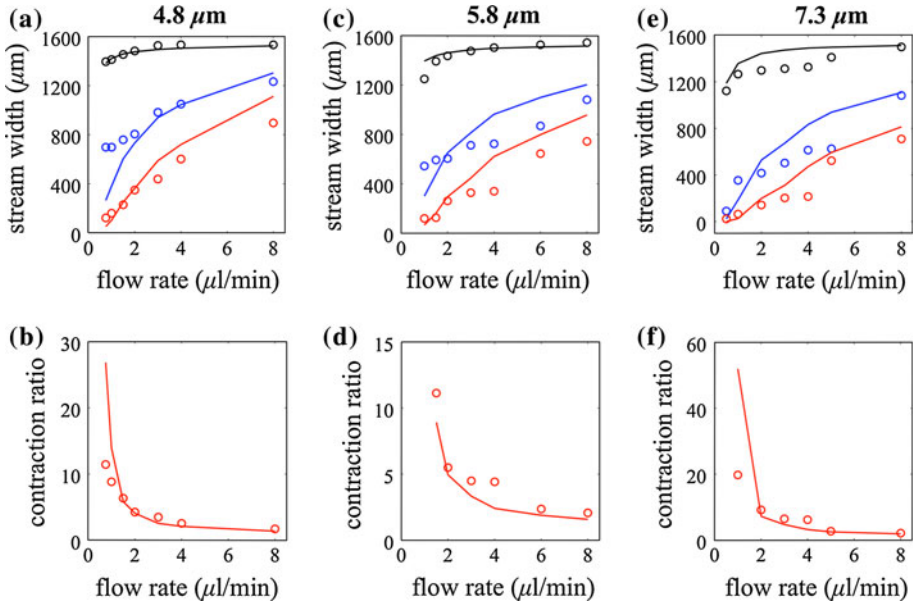

Fig. 4 Comparisons of theoretical (*solid lines*) and experimental (*circular marks*) stream widths (**a**, **c**, **e**) and contraction ratios (**b**, **d**, **f**) of 4.8 μm (**a**, **b**), 5.8 μm (**c**, **d**), and 7.3 μm (**e**, **f**) particles at various flow rates. *Top lines* and *circles* in (**a**, **c**, **e**) correspond to observation region II; *middle* ones region III; and *bottom* ones region IV. The width of particles stream decreases as the particle diameter increases, and as the flow rate decreases. As a result, contraction ratio increases as particle diameter increases, and as flow rate decreases. Discrepancy between theoretical and experimental results may be attributed to combinations of "wall" effect and finite experimental width of particles stream

reasons including "wall" effect (Staben et al. 2003) on motions of the particles and finite width of particles stream obtained from record images.

4 Conclusion

In conclusion, we have developed a novel magnetic manipulation technique and its analytical model based on ferrofluids for microparticles focusing inside a microfluidic channel. In comparison to other particle-focusing techniques, including hydrodynamic, electrokinetic, optical, dielectrophoretic, and acoustic focusing, this method is simple, low-cost, and label-free. The construction of our device is extremely simple, and we choose permanent magnet based device configurations because they eliminate complex microfabrication process and auxiliary power supply. The devices are easy to operate and do not generate heat. Microparticles do not require labeling steps because their surrounding media, ferrofluids, are magnetic by themselves. The ferrofluid used in this method are colloidal suspensions of iron oxide nanoparticles, which have reduced interferences with biological processes of samples compared to paramagnetic salt solutions. With recent developments of bio-compatible ferrofluids (Kose et al. 2009; Krebs et al. 2009; Bajaj et al. 2009), this technique can also be applied toward cell focusing and manipulation. Although ferrofluids are generally opaque, making observations of samples motion within ferrofluids challenging, we expect the advantages of this technique will eventually outweigh its disadvantages, enabling a variety of microfluidic biological and chemical applications.

Acknowledgments This research was financially supported by the Office of the Vice President for Research at the University of Georgia, and by the Centers for Disease Control and Prevention.

References

Adair RK (1991) Constraints on biological effects of weak extremely-low-frequency electromagnetic-fields. Phys Rev A 43(2):1039–1048

Afshar R, Moser Y, Lehnert T, Gijs MAM (2011) Three-dimensional magnetic focusing of superparamagnetic beads for on-chip agglutination assays. Anal Chem 83(3):1022–1029. doi:10.1021/Ac102813x

Bajaj A, Samanta B, Yan HH, Jerry DJ, Rotello VM (2009) Stability, toxicity and differential cellular uptake of protein passivated-Fe_3O_4 nanoparticles. J Mater Chem 19(35):6328–6331. doi:10.1039/B901616c

Chung TD, Kim HC (2007) Recent advances in miniaturized microfluidic flow cytometry for clinical use. Electrophoresis 28(24):4511–4520. doi:10.1002/Elps.200700620

Gijs MAM, Lacharme F, Lehmann U (2010) Microfluidic applications of magnetic particles for biological analysis and catalysis. Chem Rev 110(3):1518–1563

Gossett DR, Weaver WM, Mach AJ, Hur SC, Tse HTK, Lee W, Amini H, Di Carlo D (2010) Label-free cell separation and sorting in microfluidic systems. Anal Bioanal Chem 397(8):3249–3267

Huh D, Gu W, Kamotani Y, Grotberg JB, Takayama S (2005) Microfluidics for flow cytometric analysis of cells and particles. Physiol Meas 26(3):R73–R98. doi:10.1088/0967-3334/26/3/R02

Kose AR, Fischer B, Mao L, Koser H (2009) Label-free cellular manipulation and sorting via biocompatible ferrofluids. Proc Natl Acad Sci USA 106(51):21478–21483

Krebs MD, Erb RM, Yellen BB, Samanta B, Bajaj A, Rotello VM, Alsberg E (2009) Formation of ordered cellular structures in suspension via label-free negative magnetophoresis. Nano Lett 9(5):1812–1817

Krishnan KM (2010) Biomedical nanomagnetics: a spin through possibilities in imaging, diagnostics, and therapy. IEEE Trans Magn 46(7):2523–2558. doi:10.1109/Tmag.2010.2046907

Kummrow A, Theisen J, Frankowski M, Tuchscheerer A, Yildirim H, Brattke K, Schmidt M, Neukammer J (2009) Microfluidic structures for flow cytometric analysis of hydrodynamically focussed blood cells fabricated by ultraprecision micromachining. Lab Chip 9(7):972–981. doi:10.1039/B808336c

Lee GB, Chang CC, Huang SB, Yang RJ (2006) The hydrodynamic focusing effect inside rectangular microchannels. J Micromech Microeng 16(5):1024–1032. doi:10.1088/0960-1317/16/5/020

Liu CX, Lagae L, Borghs G (2007) Manipulation of magnetic particles on chip by magnetophoretic actuation and dielectrophoretic levitation. Appl Phys Lett 90(18):184109

Liu C, Stakenborg T, Peeters S, Lagae L (2009) Cell manipulation with magnetic particles toward microfluidic cytometry. J Appl Phys 105(10):102011–102014

Mihajlovic G, Aledealat K, Xiong P, Von Molnar S, Field M, Sullivan GJ (2007) Magnetic characterization of a single superparamagnetic bead by phase-sensitive micro-Hall magnetometry. Appl Phys Lett 91(17):172518

Pamme N (2006) Magnetism and microfluidics. Lab Chip 6(1):24–38

Pamme N (2007) Continuous flow separations in microfluidic devices. Lab Chip 7(12):1644–1659

Pankhurst QA, Connolly J, Jones SK, Dobson J (2003) Applications of magnetic nanoparticles in biomedicine. J Phys D 36(13):R167

Pankhurst QA, Thanh NKT, Jones SK, Dobson J (2009) Progress in applications of magnetic nanoparticles in biomedicine. J Phys D 42(22):224001

Petersson F, Nilsson A, Holm C, Jonsson H, Laurell T (2005) Continuous separation of lipid particles from erythrocytes by means of laminar flow and acoustic standing wave forces. Lab Chip 5(1):20–22. doi:10.1039/B405748c

Peyman SA, Iwan EY, Margarson O, Iles A, Pamme N (2009) Diamagnetic repulsion—a versatile tool for label-free particle handling in microfluidic devices. J Chromatogr A 1216(52):9055–9062

Rodriguez-Villarreal AI, Tarn MD, Madden LA, Lutz JB, Greenman J, Samitier J, Pamme N (2011) Flow focussing of particles and cells based on their intrinsic properties using a simple diamagnetic repulsion setup. Lab Chip 11(7):1240–1248. doi:10.1039/C0lc00464b

Rosensweig RE (1966) Fluidmagnetic buoyancy. AIAA J 4:1751–1758

Rosensweig RE (1985) Ferrohydrodynamics. Cambridge University Press, Cambridge

Shevkoplyas SS, Siegel AC, Westervelt RM, Prentiss MG, Whitesides GM (2007) The force acting on a superparamagnetic bead due to an applied magnetic field. Lab Chip 7(10):1294–1302. doi:10.1039/B705045c

Shi JJ, Mao XL, Ahmed D, Colletti A, Huang TJ (2008) Focusing microparticles in a microfluidic channel with standing surface

acoustic waves (SSAW). Lab Chip 8(2):221–223. doi:10.1039/B716321e

Staben ME, Zinchenko AZ, Davis RH (2003) Motion of a particle between two parallel plane walls in low-Reynolds-number Poiseuille flow. Phys Fluids 15(6):1711–1733

Tsutsui H, Ho CM (2009) Cell separation by non-inertial force fields in microfluidic systems. Mech Res Commun 36(1):92–103

Wang L, Flanagan LA, Jeon NL, Monuki E, Lee AP (2007) Dielectrophoresis switching with vertical sidewall electrodes for microfluidic flow cytometry. Lab Chip 7(9):1114–1120. doi:10.1039/B705386j

Whitesides GM (2006) The origins and the future of microfluidics. Nature 442(7101):368–373

Xuan XC, Li DQ (2005) Focused electrophoretic motion and selected electrokinetic dispensing of particles and cells in cross-micro-channels. Electrophoresis 26(18):3552–3560. doi:10.1002/Elps.200500298

Xuan XC, Zhu JJ, Church C (2010) Particle focusing in microfluidic devices. Microfluid Nanofluid 9(1):1–16. doi:10.1007/S10404-010-0602-7

Yellen BB, Hovorka O, Friedman G (2005) Arranging matter by magnetic nanoparticle assemblers. Proc Natl Acad Sci USA 102(25):8860–8864

Zhao YQ, Fujimoto BS, Jeffries GDM, Schiro PG, Chiu DT (2007) Optical gradient flow focusing. Optics Express 15(10):6167–6176

Zhu JJ, Xuan XC (2009) Dielectrophoretic focusing of particles in a microchannel constriction using DC-biased AC electric fields. Electrophoresis 30(15):2668–2675. doi:10.1002/Elps.200900017

Zhu TT, Marrero F, Mao LD (2010) Continuous separation of non-magnetic particles inside ferrofluids. Microfluid Nanofluid 9(4–5):1003–1009

Zhu T, Lichlyter D, Haidekker M, Mao L (2011) Analytical model of microfluidic transport of non-magnetic particles in ferrofluids under the influence of a permanent magnet. Microfluidics Nanofluidics 1–13. doi:10.1007/s10404-010-0754-5